Peripheral Nervous System Modulation with Wireless Cellular Sized Freestanding Injectable Devices

by

Preet Patel

B.Tech, Indian Institute of Technology Kanpur (2022)

Submitted to the Program in Media Arts and Sciences,
School of Architecture and Planning,
in partial fulfillment of the requirements for the degree of

Master of Science in Media Arts and Sciences

at the

MASSACHUSETTS INSTITUTE OF TECHNOLOGY

May 2024

©2024 Preet Patel. All rights reserved

The author hereby grants to MIT a nonexclusive, worldwide, irrevocable, royalty-free license to exercise any and all rights under copyright, including to reproduce, preserve, distribute and publicly display copies of the thesis, or release the thesis under an open-access license.

Author____

Preet Patel
Program in Media Arts and Sciences
May 24, 2024

Certified by____

Deblina Sarkar
Assistant Professor
Program in Media Arts and Sciences
Thesis Supervisor

Accepted by____

Joseph Paradiso
Academic Head, Media Arts and Sciences
Program in Media Arts and Sciences

Peripheral Nervous System Modulation with Wireless Cellular Sized Freestanding Injectable Devices

by

Preet Patel

Submitted to the Program in Media Arts and Sciences,
School of Architecture and Planning,
on May 24, 2024, in partial fulfillment of the
requirements for the degree of
Master of Science in Media Arts and Sciences

Abstract

Designing novel neural interfaces is essential for various medical applications, scientific research, and human augmentation. One of the foundations of neural interface and bioelectronic medicine is the electrical stimulation of excitable cells, to interface the body with electronics and treat a variety of diseases. Current technologies, while efficacious, are limited by their bulkiness, require highly invasive surgeries, are unable to target at single-cell level resolution and are prone to foreign body reactions. Optogenetics can address these issues but fundamentally requires genetic modifications which makes it difficult to implement in-vivo and has issues of muscle atrophy and toxicity specifically in the Peripheral Nervous System (PNS).

This work aims to advance bioelectronic medicine by developing efficient, wireless, cellular-sized electronic devices that can be administered in a drug-like fashion. These innovative, substrate-free nanoelectronic devices, termed injectable electronics, can be activated, and controlled using near-infrared (NIR) light, enabling minimally invasive, targeted neuromodulation deep within the peripheral nervous system (PNS). By overcoming the limitations of current implantable devices, this groundbreaking approach has the potential to transform the way we diagnose and treat a wide range of neurological disorders.

Thesis Supervisor: Deblina Sarkar
Title: Assistant Professor, Program in Media Arts and Sciences

Peripheral Nervous System Modulation with Wireless Cellular Sized Freestanding Injectable Devices

by

Preet Patel

The following people served as readers for this thesis:

Thesis Advisor____

Deblina Sarkar
Assistant Professor of Media Arts and Sciences
MIT Media Lab

Thesis Reader____

Hugh Herr
Professor of Media Arts and Sciences
MIT Media Lab

Thesis Reader____

Cardinal Warde
Professor of Electrical Engineering
MIT EECS

Acknowledgments

I am deeply grateful to my research advisor, Professor Deblina Sarkar, for her invaluable guidance, mentorship, and unwavering support throughout my Master's degree program. Her expertise, dedication, and commitment to my academic and professional growth have been instrumental in shaping this work. I am truly honored to have had the opportunity to work under her supervision.

I would also like to express my sincere appreciation to Professor Hugh Herr, my second advisor, for his insightful feedback, providing access to the resources and facilities that were essential for the successful completion of this thesis and funding my work through K. Lisa Yang Bionic Center. Furthermore, I would like to extend my heartfelt gratitude to Professor Warde, my thesis reader, for their valuable time, constructive criticism, thoughtful suggestions, and teaching me the ropes of optics in his class.

I am thankful to my lab members for their camaraderie, intellectual discourse, and for creating a supportive and collaborative environment. Their assistance and willingness to share their knowledge and expertise have been invaluable throughout this journey.

Finally, I would like to acknowledge the unwavering love and support of my family, who have been my constant source of strength and motivation. Their encouragement and belief in me have been the driving force behind my achievements.

Contents

List of Figures

Chapter 1

Introduction

1.1 Background

Designing novel neural interfaces is essential for various medical applications, scientific research, and human augmentation[1, 2]. One of the foundations of neural interface and bioelectronic medicine is the electrical stimulation of excitable cells, to interface the body with electronics and treat a variety of diseases. Clinically, direct electrical actuation of the nervous system is used in various medical procedures such as deep brain stimulation[3], prosthetic retinal implants[4], and vagus-nerve stimulation[5] and other disorders[6, 7]. Additionally, this method is being explored in numerous other applications, and the list of emerging technologies in the preclinical stage continues to expand consistently[8, 9].

At present, non-genetic neural stimulation encounters two main challenges. The first category involves tethered methods that demand invasive surgery[10], such as the use of electrodes/cuff electrodes and MEA (microelectrode arrays). These devices, while useful, often suffer from limitations specifically for peripheral nervous system (PNS) such as low selectivity, potential for nerve damage, and the inability to provide fine, controlled interactions with nerve fibers. For instance, cuff electrodes[11] can apply pressure to nerves, potentially leading to nerve injury or scarring over time. Moreover, nerve guidance conduits[11], used for nerve regeneration, do not always effectively support the alignment and directional growth of nerve fibers across injury gaps, which is crucial for functional recovery.

The second category consists of untethered approaches that lack cellular precision[12], example techniques like MRI. Additionally, there are modalities that fall between these two categories in terms of invasiveness. These methods entail the implantation of devices inside brain tissue or around the nerves innervating various organs, which can be wirelessly activated using various fields, including acoustic[13], magnetic[14], electromagnetic (including RF)[15], and light[16]. However, current technologies in this realm are either invasive or unable to achieve precise spatio-temporal stimulation[17].

To overcome these limitations, we need new technology which is 1) wireless and can be controlled remotely which makes it minimally invasive and 2) is cellular in size so that it can achieve single cell level resolution for stimulation, thus can be administered via injection in drug like manner. To achieve this goal of injectable electronic medicine, I am working on developing highly efficient cellular sized photovoltaic (PV) devices which can induce system level stimulation for applications in Peripheral Nervous System. These devices are 1) cellular in size (10-40µm diameter), 2) Substrate free in freestanding form, hence can be injected in a suspension, 3) are based on organic semiconducting polymers which operate selectively on near-infrared (NIR) wavelength which can penetrate deep inside the tissue and activate the device.

The key advantages of the proposed injectable electronic devices compared to current neuromodulation technologies are:

1) Minimally invasive delivery via injection, avoiding surgical implantation 2) Ability to disperse devices in 3D throughout the nerve for high spatial resolution 3) Close and stable interfacing with individual axons enabled by the small, flexible form factor 4) Reduced foreign body response and improved long-term stability

These injectable electronic devices have the potential to treat several diseases through precise peripheral nerve modulation, including:

1. Type 1 diabetes: Vagus nerve stimulation using injectable electronic devices could potentially help manage type 1 diabetes[5] by regulating glucose metabolism.

2. Rheumatoid arthritis: Stimulation of the splenic nerve using injectable electronics is a potential treatment approach for rheumatoid arthritis[18] by reducing systemic inflammation.

3. Neuropathic pain: Precise modulation of peripheral nerves involved in pain signaling, using injectable devices could provide a targeted approach to treating neuropathic pain conditions [19].

4. Muscle control disorders: Injectable electronic interfaces with motor nerves could enable more naturalistic and selective control of muscle activation for treating paralysis, spasticity, or muscle weakness [20].

In summary, while established neuromodulation techniques can already address some of these disease indications to an extent, injectable electronics could provide a more precise, stable, and clinically translatable solution for peripheral nerve modulation therapies. The current focus of this thesis is on the development of these devices for Peripheral Nervous System (PNS) modulation. However, significant preclinical and clinical testing will be required to validate their safety and efficacy before realizing their full potential in bioelectronic medicine

1.2 Organic Photovoltaics (OPVs): Overview and Functionality

Organic Photovoltaics (OPVs)[21] represent a class of solar cell technologies that utilize organic molecules or polymers to convert sunlight into electricity. Unlike traditional photovoltaic technologies that often use inorganic materials such as silicon, OPVs involve organic compounds which are carbon-based. These materials are capable of absorbing light and facilitating the flow of electrical charges.

1.2.1 Functioning of OPVs

The basic operational mechanism of an OPV involves several key steps:

1. Light Absorption: When light is incident on the organic active layer, the photons are absorbed, exciting electrons from the highest occupied molecular orbital (HOMO) to the lowest unoccupied molecular orbital (LUMO) of the organic semiconductor. This process generates bound electron-hole pairs called excitons.
2. Exciton diffusion: The generated excitons diffuse through the organic layer towards an interface between two organic materials - an electron donor and an electron acceptor. This interface is critical for charge separation.
3. Charge separation: At the donor-acceptor interface, the excitons dissociate into free charge carriers - electrons and holes. The LUMO level offset between the donor and acceptor provides the driving force for this dissociation. Electrons transfer to the acceptor material while holes remain in the donor.
4. Charge transport and collection: The separated free charges then transport through the respective donor and acceptor materials towards the electrodes, driven by the built-in electric field. Electrons are collected at the low work function cathode (often a metal like aluminum), while holes are collected at the high work function anode (often a transparent conductive oxide like indium tin oxide).

The OPV active layer is typically sandwiched between these two electrodes to form a complete photovoltaic cell. An important aspect of OPV cell design is morphology control of the donor-acceptor blend to ensure efficient exciton dissociation and charge transport pathways to the electrodes.

Some key characteristics of the organic semiconductors enable this photovoltaic function:

- The conjugated π-electron system allows absorption of light to generate excitons

- The offset between donor and acceptor energy levels enables exciton dissociation into free charges
- The semiconducting properties allow transport of free charges to be extracted as current

1.2.2 Structural Components

An OPV typically consists of several layers, each contributing to the device's functionality:

- Transparent Electrode: Usually positioned on the top layer to allow sunlight to enter the device while also collecting and transporting charges.
- Active Layer: Composed of the donor and acceptor materials where light absorption, exciton formation, and charge separation occur.
- Electron or Hole Transport Layers: These layers help in the efficient transport of electrons and holes to their respective electrodes, minimizing recombination losses.
- Metal Electrode: Serves as the counter electrode, collecting charges of opposite type to those collected by the transparent electrode.

In summary, OPV cells convert light to electricity through a process of light absorption in organic semiconductors, exciton generation and diffusion, charge separation at donor-acceptor interfaces, and charge transport and extraction at electrodes. Precise control over materials design and device engineering is critical to optimize each of these steps for high performance. The unique properties of organic materials, such as tunable electronic and optical properties and solution processability, flexibility and low costs [21] make OPVs a versatile and potentially transformative technology for optoelectronic biomedical applications.

1.3 Thesis Objectives

The primary objective of this thesis is to develop and characterize highly efficient, cellular-sized, freestanding photovoltaic (PV) devices for minimally invasive and precise neural stimulation in the peripheral nervous system (PNS). The specific goals are as follows:

1.3.1 Device Fabrication, Characterization and Further Optimizations

* Design and fabricate PV devices with a vertical architecture consisting of an anode, an organic semiconducting polymer, and a cathode on a silicon substrate.

* Explore various electrode materials, such as PEDOT:PSS, Platinum, Platinum Iridium, Titanium, and Titanium Nitride, and investigate different bulk heterojunction combinations to optimize device performance.

* Employ advanced fabrication techniques, including spin-coating, photolithography, Physical Vapor Deposition (PVD), and ICP-RIE (Reactive Ion Etching), to create high-quality, cellular-sized (10 to 40 µm) devices in a cleanroom environment.

* Release the devices from the Si-Wafer substrate using a sacrificial layer and characterize them using SEM and a custom two-probe setup for electrical characterization.

1.3.2 Testing Free Standing Devices in real biological working environment with an artificial cell membrane

Evaluate the performance of the PV devices within a controlled biological setting. This includes designing experiments using lipid bilayer membranes to mimic neuronal cell membranes and assessing the devices' ability to modulate neural activity through it's ability to generate potential across the artificial membrane.

1.3.3 In Vivo Experiments

* Demonstrate the application of the PV devices in PNS stimulation using BALB/c mice.

* Perform acute in vivo sciatic nerve biomodulation by injecting cellular-sized PV devices directly into the sciatic nerve, allowing access to all fascicles.

* Utilize two experimental setups: focusing the laser beam directly on the exposed nerve and focusing the laser from outside through skin and muscle/fat tissues to the nerve.

* Characterize the stimulation response using multi-channel electromyography (EMG) recordings from gastrocnemius medialis, tibialis anterior, and plantar interossei muscles innervated by the sciatic nerve to study muscle activation and selectivity.

1.4 Thesis Organization

The rest of the Thesis is organized as follows:

Chapter 2 delves into the design principles and fabrication processes of the photovoltaic devices. Further discussions on material selection, layer deposition, and device optimization strategies.

In Chapter 3 electrical properties of the devices are thoroughly examined. It presents the characterization techniques used to evaluate device performance both on substrates and in a freestanding form. Additionally, this chapter explores the interaction of these devices in free standing form with artificial cell membranes, simulating a biological environment to assess their functional capabilities.

Chapter 4 discusses the current In Vivo Peripheral Nervous System Modulation experiment. It covers the methodologies for injecting the devices into the sciatic nerve of animal models and discusses the preliminary findings from these in vivo experiments. The chapter concludes with an overview of the progress made in animal studies and outlines the future directions for this line of research.

Chapter 2

Device Design and Fabrication for Injectable electronics

2.1 Introduction

Photovoltaic (PV) devices are a promising technology in the realm of neural stimulation, leveraging light to interface with the intricacies of the nervous system [22]. In pursuit of developing injectable electronics for peripheral nervous system modulation, this chapter delves into the critical aspects of designing and fabricating cellular-sized, freestanding PV devices. Specifically, we will explore the material selection, nano-fabrication techniques, and device optimization strategies that enable the miniaturization of conventional PV devices to achieve efficient neuromodulation at the single-cell level.

2.2 Design Principles and Material Selection

Designing organic photovoltaic (OPV) devices for biomedical applications at cellular spatial resolutions presents unique challenges in the fabrication process. The constraints inherent in fabricating devices at this scale limit the direct translation of efficiencies achieved in standard OPVs used for energy harvesting. Factors contributing to the power conversion efficiency (PCE) of these devices include the combination of active polymers (acceptors and donors) used for photocurrent generation, electron transport layers (ETL) and hole transport layers (HTL) for efficient electron-hole pair separation, and the choice of efficient electrodes, which influence the photo-potential and recombination rates.

2.2.1 Device Architecture

The device architecture is a vertical stack of materials comprising an anode poly(3,4-ethylenedioxythiophene) polystyrene sulfonate (PEDOT:PSS), an organic semiconducting layer of donor polymer and acceptor material, a cathode (titanium), and a neural stimulation electrode (titanium nitride). This arrangement is precisely fabricated on a silicon substrate. The selection of electrodes is guided by the necessity for a defined built-in electric field, transparency, and charge injection capacity.

2.2.2 Anode: PEDOT:PSS

Poly(3,4-ethylenedioxythiophene) polystyrene sulfonate (PEDOT:PSS)[23], a transparent conducting polymer, is chosen as the anode due to its high work function (around 5.0 eV), which facilitates efficient hole extraction from the active layer. PEDOT:PSS is widely used in bioelectronics due to its unique combination of electrical conductivity, optical transparency, and biocompatibility. Its ability to conduct both ionic and electronic charges makes it particularly suitable for interfacing with biological systems. PEDOT:PSS has been extensively studied for various biomedical applications, including neural electrodes, biosensors, and tissue engineering scaffolds. Its flexibility and mechanical stability also enable seamless integration with soft biological tissues.

2.2.3 Cathode: Titanium

Titanium is selected as the cathode material because of its low work function (around 4.3 eV), which enables efficient electron collection from the active layer. Moreover, titanium's biocompatibility and stability in biological environments make it an ideal choice for this application.

2.2.4 Stimulation Electrode layer: Titanium Nitride

To further enhance the neural stimulation capabilities of the device, a layer of titanium nitride (TiN) is deposited on top of the titanium cathode. TiN[24, 25] is a well-established material for neural stimulation due to its high charge injection capacity, low impedance, and excellent biocompatibility. The incorporation of TiN as the stimulating electrode ensures efficient charge transfer between the device and the target neurons, facilitating effective neuromodulation.

2.2.5 Active Layer: Bulk Heterojunction / Organic Semi-Conducting polymers

The choice of the organic semiconducting polymer blend is dictated by the desired operating wavelength and the targeted efficiency of the device. This blend is a bulk heterojunction system that exhibits strong absorption in the near-infrared (NIR) region, which is crucial for neuromodulation applications as NIR light can penetrate biological tissues effectively. The combination of the donor polymer and the acceptor material enhances charge separation and transport, leading to improved device performance.

2.2.6 Summary

In summary, the OPV device stack featuring PEDOT:PSS/organic semiconducting polymer blend/Titanium/Titanium Nitride is designed to optimize the performance of OPVs for applications requiring near-infrared (NIR) light absorption and biocompatibility, such as in-vitro and in-vivo neuromodulation. The carefully selected materials and their specific roles in the device architecture contribute to efficient charge generation, separation, and collection, ultimately enabling effective neural stimulation at cellular spatial resolutions.

2.3 Device Fabrication

The fabrication of these devices was carried out on two different substrates: Glass Chip coated with ITO (Indium Tin Oxide) [25mm X 25mm] and Si wafer [4 inch]. The ITO-coated glass substrates were employed for device characterization, while the Si substrates were utilized for the lift-off process and subsequent stimulation experiments. Prior to the spin-coating process, the Si substrate was coated with a layer of Ti (100 nm) followed by Al (200 nm). The overall fabrication process, as illustrated in Fig. 2-1, can be divided into several key stages, which will be discussed in the following subsections.

2.3.1 Preparing the Substrate

Depositing the Ti-Al Sacrificial Layer

For devices fabricated on Si wafers, a sacrificial layer was deposited before the device material stack. The Si wafers underwent a pre-cleaning step using an Oxygen Plasma treatment (100W for 30 seconds) in a Plasma Asher. Following this, the wafers were transferred to an Electron Beam deposition system. The chamber was evacuated to achieve a base vacuum level of 1.5×10^{-6} torr. Subsequently, the desired materials (Titanium and Aluminum) were deposited at a controlled rate of 1 Å/s while the wafers were rotated to ensure a uniform coating. The deposition process was carried out at an elevated temperature of 50°C. The Titanium layer served as a back contact for electrochemical reactions, while the Aluminum layer acted as a sacrificial layer for the subsequent lift-off process.

To prepare the ITO substrates for spin coating, begin by thoroughly cleaning them with a soap solution. Subsequently, subject the substrates to sequential ultrasonication in DI

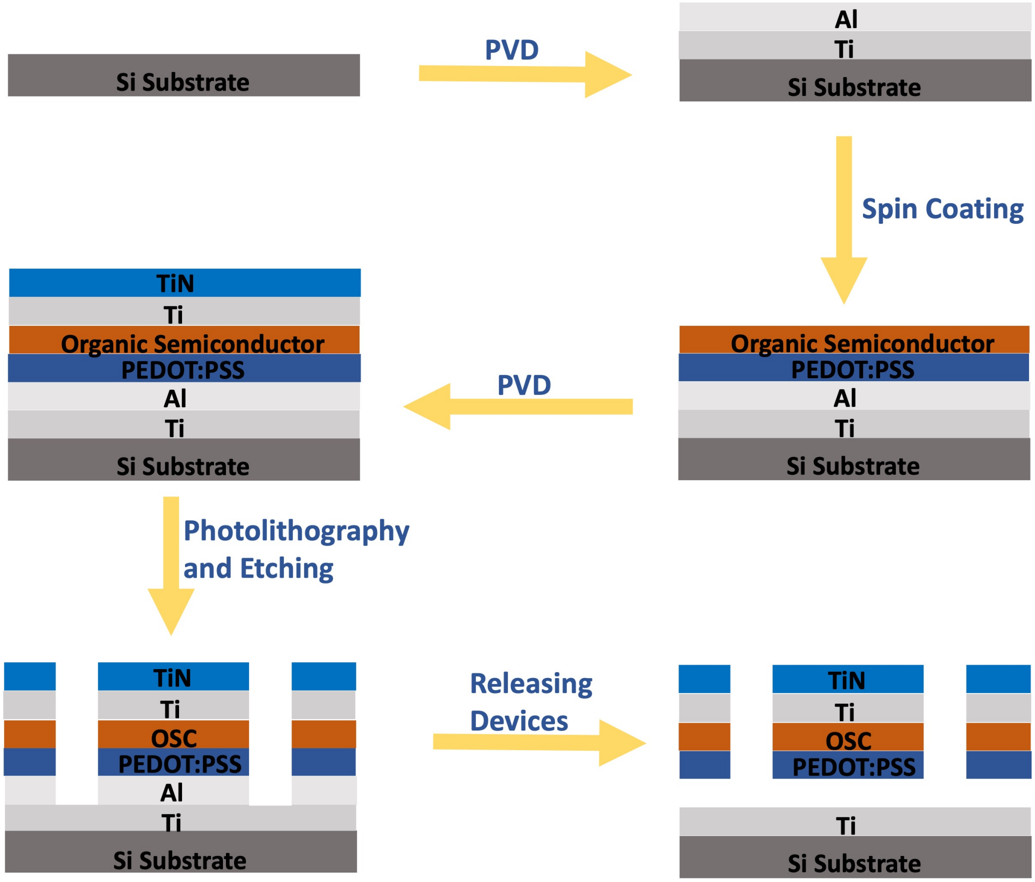

Figure 2-1: Fabrication Process Schematic

water, acetone, and IPA for 10 minutes each. After the cleaning process, use a nitrogen gun to dry the substrates and then expose them to a UV lamp for UV ozonization. Prior to the spin coating process, both the ITO and Si substrates should undergo an oxygen plasma treatment. This step is crucial for de-wetting and cleaning the surface of the substrates. Apply the oxygen plasma at a power of 200W for a duration of 1 minute to ensure optimal surface preparation.

2.3.2 Polymer Preparation

To ensure optimal performance of the PEDOT:PSS layer, it is essential to filter the solution using 0.22um PTFE filters prior to further processing. Once filtered, the PEDOT:PSS solution is modified by incorporating 5% DMSO, 0.2% GOPS, and 0.1% Dynol 604. These additives are thoroughly mixed into the solution by stirring for 20 minutes. DMSO serves to enhance the morphology and conductivity of the PEDOT:PSS layer, while GOPS imparts stability and renders the layer insoluble in water-based solutions. Additionally, Dynol 604 is included to increase the hydrophilicity of the PEDOT:PSS layer. After the mixing process, the solution undergoes a final filtration step using a 0.45um PTFE filter to remove any remaining particulates before spin coating.

The preparation of the active layer polymer blend takes place inside a glovebox environment to maintain an inert atmosphere. The polymer blend solution is prepared a day in advance and allowed to stir overnight to ensure complete dissolution. Dichlorobenzene is employed as the solvent for this solution, with a donor-to-acceptor ratio of 1:1 and an overall concentration of 20mg/ml. To facilitate the dissolution process, the dichlorobenzene is heated to 100°C while stirring. The dissolution process typically takes no more than 10-12 hours at elevated temperatures. Prior to spin coating, the polymer blend solution is filtered using 0.45um PTFE filters to remove any undissolved particles or aggregates.

2.3.3 Spin Coating

After the de-wetting process, the subsequent steps involved the spin coating of polymers onto the substrates. The PEDOT:PSS layer was deposited outside the glovebox environment by spin coating at a speed of 1000 rpm, followed by annealing at 120°C for 10 minutes. This procedure resulted in the formation of a 100 nm thick PEDOT:PSS layer. Upon completion of the annealing step, the substrates were carefully transferred into the glovebox. Inside the glovebox, the organic semiconducting polymer blend solution was spin-coated onto the PEDOT:PSS pre-coated substrates at a speed of 800 rpm for a duration of 1 minute. To ensure proper film formation and solvent evaporation, the polymer blend layer was then annealed at 140°C for 5 minutes. Through this spin coating and annealing process, a uniform thin film of the polymer blend with a thickness of 220 nm was successfully deposited on top of the PEDOT:PSS layer.

2.3.4 Top Layer Deposition

Following the spin coating of the active layers, the devices were carefully sealed and transported to the cleanroom facility at MIT.nano for the deposition of the top metal electrode. The sealed devices were placed inside the vacuum chamber of the electron beam (E-beam) deposition system. The chamber was then evacuated until the pressure reached a level of 10^{-7} torr, ensuring a clean and contaminant-free environment for the deposition process. Once the desired vacuum level was achieved, the top metal electrode, consisting of titanium (Ti), was deposited onto the active layers. The thickness of the Ti layer was precisely controlled to 50 nm, and the deposition rate was maintained at a steady 1 Å/s to ensure a uniform and high-quality electrode formation.

After the deposition of the titanium layer, the wafer was transferred to a sputtering tool for the subsequent deposition of titanium nitride (TiN). The sputtering chamber was evacuated to a base pressure of $3\text{x}10^{-6}$ torr to ensure a clean environment for the deposition process. Once the desired vacuum level was achieved, the chamber was supplied with a mixture of gases: 9 sccm of argon (Ar) and 3 sccm of nitrogen (N_2). The sputtering target used in this process was titanium (Ti).

When the RF (radio frequency) power was applied to the sputtering gun, the titanium target was bombarded with high-energy ions generated from the argon plasma. This bombardment caused the ejection of titanium atoms from the target surface. Simultaneously, the nitrogen gas present in the chamber reacted with the ejected titanium atoms, forming titanium nitride (TiN) compounds. These TiN compounds then condensed and deposited onto the wafer surface, creating a uniform layer of TiN. The deposition rate was carefully controlled at 0.25 Å/s, resulting in the formation of a 30 nm thick TiN layer on top of the previously deposited titanium layer.

2.3.5 Photolithography

Following the deposition of the metal layers, the substrate underwent an annealing process at 100°C for 30 minutes to remove any residual moisture, a critical step for the subsequent application of photoresist. To fabricate individual devices of varying shapes and sizes, photolithography was employed. For this, a positive photoresist (AZ3312) was spin-coated at 3000 rpm to achieve a consistent layer thickness of 1 micron. This layer was then pre-baked at 100°C for 1 minute to stabilize the photoresist.

The patterning of the devices was performed using the MLA150 laser writer. The design for the masks used in this process was generated with KLayout software. The exposure dose set for the MLA150 was 130 mJ/cm^2 at a wavelength of 365 nm. Following the laser exposure, a post-bake was conducted at 100°C for 1 minute on a hotplate to further cure the photoresist. The development of the pattern was carried out using AZ300 MIF developer, immersing the substrates for 1 minute, followed by a rinse in water and drying with a nitrogen gun to remove any remaining developer and moisture.

The integrity and accuracy of the pattern were then inspected under an optical microscope to confirm the success of the lithography process. Finally, the wafers were subjected to a hard bake at 100°C for 30 minutes to further solidify the photoresist in preparation for subsequent processing steps.

2.3.6 Etching

After the photolithography step, the substrate features multiple polymer layers spin-coated across the entire wafer, with the patterned photoresist (PR) on top. To create devices with the desired shapes and sizes, reactive ion etching (RIE) is employed to selectively remove the targeted materials, such as titanium (Ti) and organic polymers, from the unwanted areas.

RIE is a dry etching technique that utilizes chemically reactive plasma to remove material from the substrate surface. It offers advantages over wet etching, including better anisotropy, improved uniformity, and higher resolution. By carefully selecting the etching chemistry, gas flow rates, chamber pressure, and RF power, highly controlled and selective etching of the target materials can be achieved.

In the fabrication process, various etching recipes (O_2, Cl, and F chemistries) were tried to determine the optimal conditions. SF_6-based chemistry provided the best results for Ti/TiN etching. After Ti/TiN etching, the burnt photoresist residue was removed by rinsing the wafers in acetone and sonicating for 5 minutes. Subsequently, the organic polymers were etched using oxygen plasma in the RIE tool for 5 minutes, effectively removing the unwanted areas while preserving the desired device patterns.

By employing RIE techniques, we successfully fabricated cellular-sized photovoltaic devices with precise control over their shapes and sizes. The combination of SF6-based chemistry for Ti/TiN etching and oxygen plasma for organic polymer removal proved to be an effective approach for achieving the desired device structures.

2.3.7 Releasing the Devices

For the devices fabricated on ITO substrates, the release process was not applicable as these devices were primarily intended for on-substrate testing. However, for the devices built on Si wafers, a TMAH-based release process was employed to detach them from the substrate. TMAH (tetramethylammonium hydroxide) is an effective etchant for aluminum and has the advantage of being selective, leaving both titanium and organic polymers unaffected, making it well-suited for our requirements.

Through experimentation, we determined that a 2% aqueous solution of TMAH was capable of dissolving the aluminum layer without compromising the integrity of the titanium top electrode. Interestingly, we discovered that the TMAH-based developer solution (AZ300MIF) used in the photolithography process did not degrade the device performance, leading us to adopt this chemical for the release process as well.

After conducting thorough performance characterization, we confirmed that the TMAH-based release process effectively detached the devices from the Si substrate without any detrimental effects on their functionality. In the next chapter SEM images of the devices on substrate and released devices are presented.

2.3.8 Collection of Released Devices

Following the successful release of the devices, efficient collection is a crucial step to maximize the yield, as our CMOS-compatible fabrication methods enable the production of millions of devices on a single wafer. To accomplish this, we employ a custom pump-based filtration method. A wafer is diesawed into chips and using the developer, they are released in the glass vial, giving us a suspension of devices. The suspension is then filtered using a PTFE (polytetrafluoroethylene) Nanosep filter with a pore size of 0.45µm. By applying a vacuum at one end of the filter and adding the device suspension to the other end, the developer solution is effectively removed, leaving the devices on the filter surface.

To ensure the purity of the collected devices, we perform three additional rinse cycles with deionized (DI) water using the same filtration setup. This step helps to remove any residual developer solution or contaminants that may have been present in the suspension. After the rinsing process, the devices can be easily collected in a suitable medium, such as cell culture media or phosphate-buffered saline (PBS), depending on the intended application. One of the advantages of using a PTFE filter is that the devices do not adhere to its surface, allowing for efficient recovery of the devices from the filter.

This custom filtration method not only enables the effective collection of the released devices but also provides flexibility in terms of the final suspension medium. By tailoring the collection process to the specific requirements of the downstream application, we can ensure that the devices are prepared for immediate use or further characterization. The ability to collect a large number of devices while maintaining their integrity and purity is a critical aspect of our fabrication workflow, enabling the realization of the full potential of these cellular-sized photovoltaic devices.

Chapter 3

Device Characterization

3.1 Introduction

Device characterization is an essential step in the development and optimization of cellular-sized photovoltaic devices, providing crucial insights into their physical, electrical, and functional properties. In this chapter, we present a comprehensive characterization of our devices using various techniques, including scanning electron microscopy (SEM), profilometry, current-voltage (I-V) measurements, and lipid bilayer membrane interfacing.

To gain a thorough understanding of the device morphology and dimensions, we employ SEM imaging, which offers high-resolution visualization of the fabricated structures. This technique allows us to examine the quality of the patterning process, assess the uniformity of the layers, and identify any potential defects or irregularities in the devices. Profilometry is used to measure the thickness of individual layers, ensuring desired thicknesses are achieved. Electrical characterization through I-V measurements provides insights into device performance, including open-circuit voltage, short-circuit current, fill factor etc.

To evaluate the functionality of released devices in a biologically relevant environment, we create an artificial interface using a lipid bilayer membrane, mimicking the cell membrane.

By measuring the electrical response of devices in the presence of the lipid bilayer, we assess their potential for applications such as neural stimulation.

In the following sections, we will present the experimental methods, results, and discussions for each characterization technique. Through this comprehensive characterization, we aim to demonstrate the viability and performance of our cellular-sized photovoltaic devices, paving the way for their integration into various biomedical and technological applications.

3.2 Physical Characterization

3.2.1 Optimization of Polymer Layer Thickness

The thickness of the polymer layers in our cellular-sized photovoltaic devices significantly influences their performance and efficiency. To optimize the device performance, we investigated the relationship between the spin coating parameters and the resulting polymer layer thickness.

Experimental Method

A Dektak 150 profilometer was used to measure the thickness of the polymer layers. Chips were prepared by spin coating the polymer at different rotational speeds (rpm) to obtain a range of thicknesses. After spin coating, a step profile was created in the polymer layer by gently scratching the surface with a sharp object.

Results and Discussion

The Dektak 150 profilometer scanned across the scratched region of each chip, measuring the step height between the substrate surface and the top of the polymer layer. By comparing the thickness measurements for different spin coating speeds, we established a relationship between the rpm and the resulting polymer layer thickness.

Optimizing the polymer layer thickness is crucial for several reasons. The thickness of the active layer (organic semiconducting polymer blend) influences light absorption and charge carrier generation, while the thickness of the anode (e.g., PEDOT:PSS) and the cathode (e.g., Ti) affects charge extraction, transport properties, and device stability.

By systematically varying the spin coating parameters and measuring the resulting thicknesses, we identified the optimal thickness range for each polymer layer in our device stack. This optimization process allowed us to fabricate devices with improved performance, higher efficiency, and better stability.

3.2.2 SEM Imaging

Scanning electron microscopy (SEM) imaging was employed to verify the effectiveness of the etching and lifting off processes. The Gemini 450 SEM, a high-resolution field emission scanning electron microscope at MIT.nano, was used for this purpose.

SEM imaging was performed at various stages of the fabrication process. After the reactive ion etching (RIE) process, SEM images were acquired to examine the patterned structures and ensure that the desired features were successfully transferred to the device layers. The high-resolution imaging capability of the Gemini 450 SEM allowed for the inspection of etched profiles, checking for any irregularities or unintended damage.

Following the lifting off process, SEM imaging was again employed to evaluate the released devices. High-magnification images of the freestanding structures confirmed that the devices were successfully detached from the substrate and maintained their intended shapes and dimensions. The SEM analysis also provided insights into the surface morphology and uniformity of the released devices.

The SEM imaging results confirmed the success of our etching and lifting off processes, validating the fabrication methodology for creating cellular-sized photovoltaic devices. The high-resolution images provided valuable feedback for process optimization and quality control, ensuring that the devices met the desired specifications and were suitable for subsequent characterization and application studies.

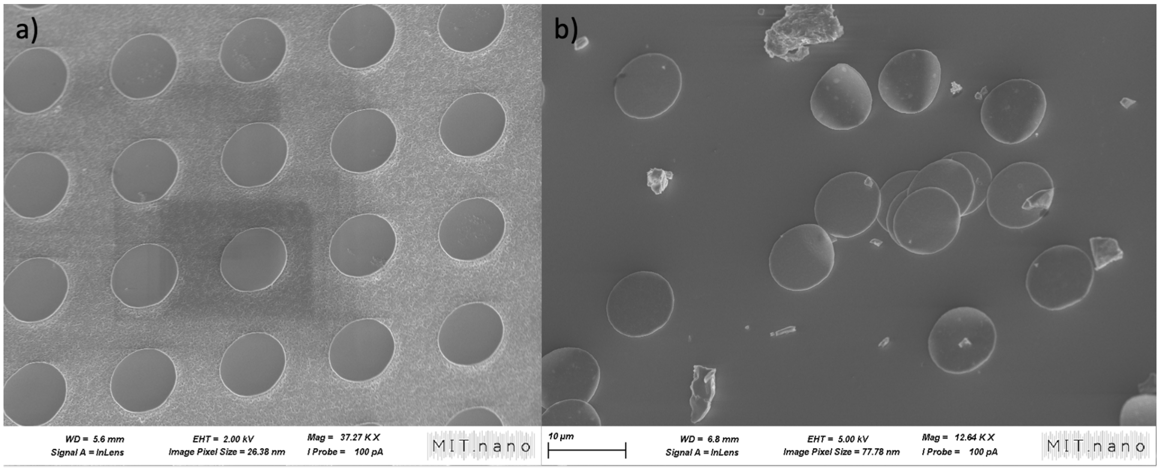

Figure 3-1: SEM Images: (a) 10µm devices on Si Wafer substrate (b) 10 µm devices released from the substrate, collected and then dropcasted for imaging

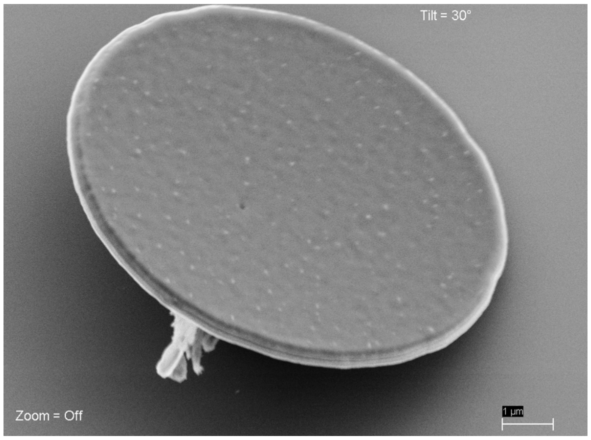

Figure 3-2: Single free standing device released from the susbstrate

3.3 Electrical Characterization

To characterize the electrical properties of our cellular-sized photovoltaic devices, we fabricated them on Glass-ITO substrates. These substrates provide a transparent and conductive platform, allowing for efficient light illumination and electrical contact. To accurately probe devices with diameters as small as 4 µm, we developed a custom-built probing station that integrates an upright microscope, precision micromanipulators, and a small window on the bottom for light illumination.

The upright microscope in the probing station enables high-magnification visualization of the devices, facilitating precise positioning of the probes. The precision micromanipulators allow for fine control over the probe placement, ensuring accurate contact with the miniaturized devices. The small window on the bottom of the setup permits light to be illuminated onto the sample devices, enabling the characterization of their photovoltaic properties.

3.3.1 Current-Voltage (I-V) Measurements

To evaluate the electrical performance of our devices, we conducted current-voltage (I-V) measurements using a potentiostat. The potentiostat applies a voltage sweep across the device and measures the resulting current, generating an I-V curve that provides valuable insights into the device characteristics.

During the I-V measurements, the devices were illuminated with a 785 nm laser, which falls within the near-infrared (NIR) region of the electromagnetic spectrum. This wavelength was chosen based on the absorption properties of the active layer materials and the transparency of biological tissues in the NIR range [26], making it suitable for potential biomedical applications.

The I-V curves obtained from the measurements reveal important device parameters such as the open-circuit voltage (Voc), short-circuit current (Isc), fill factor (FF), and power conversion efficiency (PCE). These parameters provide a comprehensive understanding of the device performance and help in optimizing the device design and fabrication process.

3.3.2 Results and Discussion

Figure 3-3 shows the I-V curve obtained from the measurements and demonstrate the successful operation of our cellular-sized photovoltaic devices. The devices exhibit clear photovoltaic behavior, with a distinct difference between the dark and illuminated I-V curves. The Voc and Isc values indicate the device's ability to generate a photovoltage and photocurrent, respectively, upon illumination with the 785 nm laser.

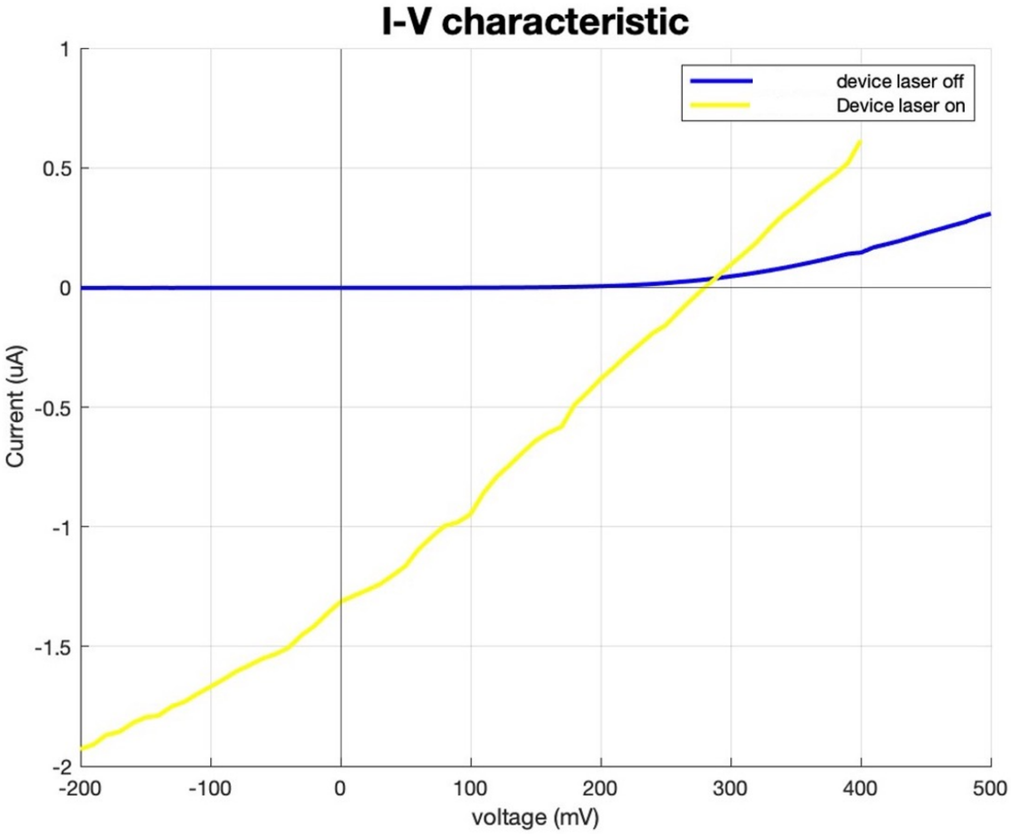

Figure 3-3: IV curve of a 40µm device for laser off and laser on; the diode curve shifts down in the fourth quadrant when the light is illuminated on it, showing power generation

The performance evaluation of our cellular-sized photovoltaic devices is facilitated by analyzing their current-voltage (I-V) characteristics and extracting key parameters. Figure 3-4 illustrates the typical electrical response of a cellular-sized device using the organic semiconducting polymer blend, revealing a short-circuit current I_{SC} of 1.5 µA and an open-circuit voltage V_{OC} of 280 mV. The electrical characterization results demonstrate the potential of these devices for applications demanding efficient, miniaturized energy conversion, such as in the biomedical field.

Notably, to achieve neuromodulation through the generation of action potentials in neuronal membranes, a change in potential across the membrane of approximately 10-15 mV is required. As depicted in Figure 3-4, our devices can attain this threshold with a light intensity, which falls within the safety limits for biological systems. This capability underscores

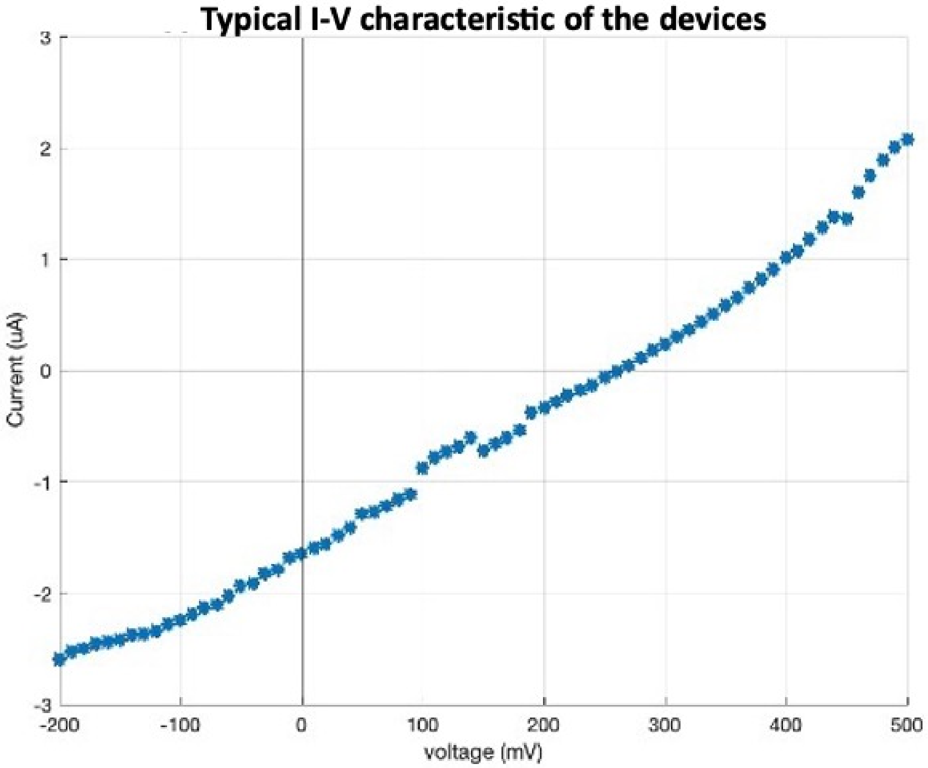

Figure 3-4: Typical IV curve for a 40µm device

the suitability of our cellular-sized photovoltaic devices for neuromodulation applications, where precise and localized stimulation is essential for therapeutic interventions or scientific investigations.

In the next section, we will discuss the integration of our devices with lipid bilayer membranes to assess their performance in a biologically relevant environment.

3.4 Testing Free Standing Devices in real biological working environment with an artificial cell membrane

To evaluate the performance of our cellular-sized photovoltaic devices in a biologically relevant environment, we designed an experiment using a lipid bilayer membrane (BLM) setup. The BLM serves as an artificial cell membrane, mimicking the capacitive properties of a neuron's cell membrane without the presence of ion channels.

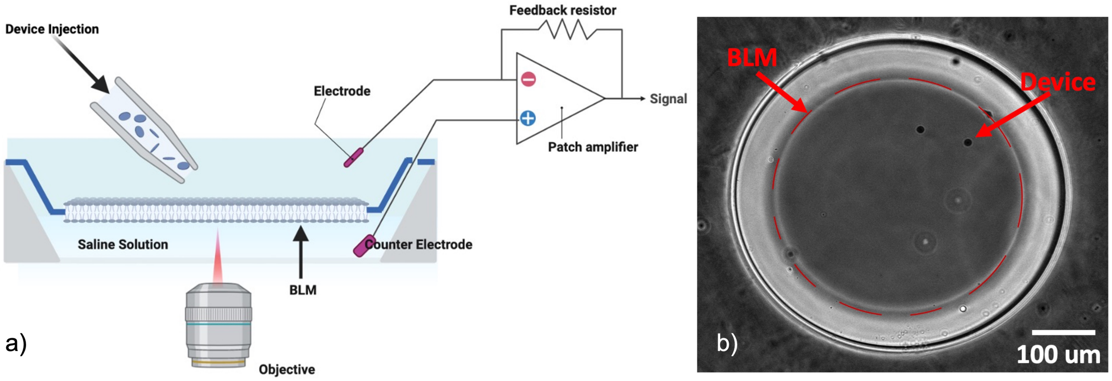

Figure 3-5: (a)Lipid Bilayer Experiment Schematic (b) BLM with devices on top

3.4.1 Experimental Setup

The BLM experiment involves the following key steps:

1. BLM Formation: A Teflon sheet with a 500 µm hole is mounted on a Teflon part using vacuum grease. A phospholipid solution (1,2-diphytanoyl-sn-glycero-3-phosphocholine in hexane) is dispensed around the hole and allowed to dry, creating a lipid monolayer.

2. Buffer Preparation: A buffer solution (1M KCl, 10mM Tris-HCl, 1mM EDTA in DI water, pH adjusted to 8.0) is introduced into a bottom teflon part, and the top part on which the teflon sheet with hole is mounted is placed in this chamber and is put on focus using a 20x microscope objective.

3. BLM Formation: A glass micropipette is filled with a phospholipid solution (1,2-diphytanoyl-sn-glycero-3-phosphocholine in decane), and a small volume is dispensed onto the aperture. The excess lipid is brushed away until vesicle-like structures are observed, and an air bubble is used to wash away any remaining excess until the BLM is formed.

4. Device Introduction: The freestanding devices are either drop-casted or injected onto the BLM using a micropump injection setup.

5. Electrical Measurements: A patch amplifier is used to measure the voltage generated across the BLM by the devices when illuminated with near-infrared (NIR) light pulses from a laser source.

3.4.2 Results and Discussion

Figure 3-5 illustrates the experimental setup for testing the freestanding devices on the BLM. The devices are introduced onto the BLM, and NIR light pulses (100 ms duration, 1 Hz frequency, 640 nm wavelength) are applied for 8 seconds.

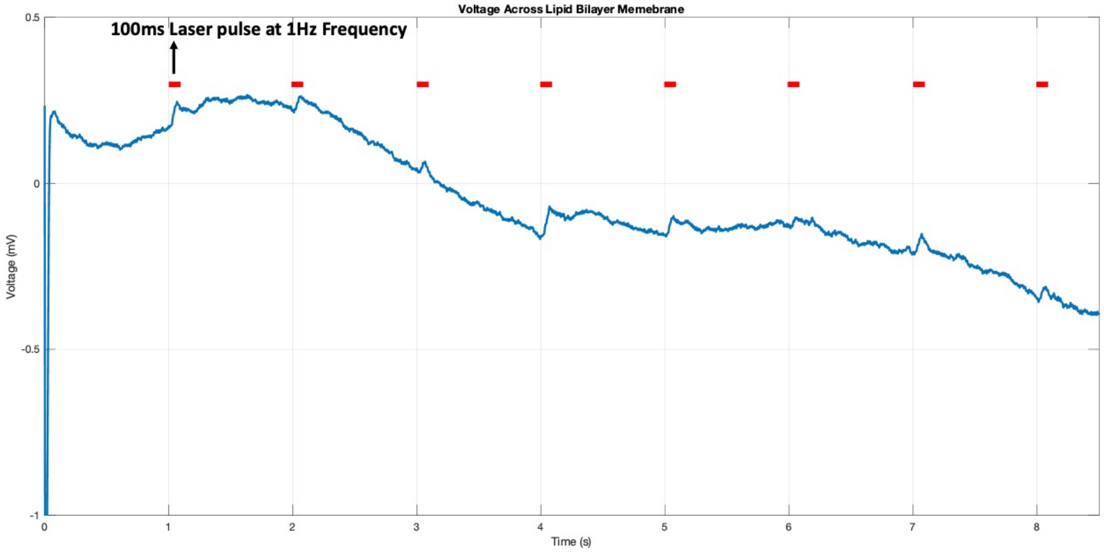

Figure 3-6: Voltage Peaks Generated across the membrane when the light pulse is illuminated

The results, as shown in Figure 3-6, demonstrate clear photovoltage peaks generated by the devices across the BLM. These peaks correspond to the light pulses (100 ms long), indicating that the devices are successfully generating a voltage response when illuminated, even in the presence of the artificial cell membrane in free standing form.

The photovoltaic devices generate a voltage of approximately 80 µV across a 300 µm diameter BLM, which serves as an artificial model of a biological membrane. However, the goal is to modulate the electrical activity of neurons, which have a much smaller diameter, typically around 10 µm. Due to the difference in size and capacitance between the BLM (0.5 µF/cm^2) and a neuronal membrane (1 µF/cm^2), the same voltage change across the BLM would result in a larger voltage change across the neuronal membrane.

Specifically, the 80 µV voltage generated across the 300 µm BLM translates to a voltage difference (ΔV) of 36 mV across a 10 µm diameter neuronal membrane. This scaling is due to the inverse relationship between membrane capacitance and voltage, where a smaller capacitance (as in the case of a neuron) results in a larger voltage change for the same amount of charge.

A voltage difference of 36 mV across a neuronal membrane is considered sufficient for neuromodulation because it exceeds the threshold for initiating an action potential in most neurons. Typically, a depolarization of the neuronal membrane by approximately 10-15 mV is required to reach the threshold potential and trigger an action potential. Therefore, a ΔV of 36 mV generated by the photovoltaic devices would be more than enough to modulate the electrical activity of neurons, either by initiating action potentials or altering the membrane potential to influence neuronal firing patterns.

This ability to induce voltage changes across neuronal membranes is crucial for applications in bioelectronic medicine, such as neural stimulation, neuromodulation therapies, and the development of brain-computer interfaces. By leveraging the photovoltaic effect at the cellular scale, these devices can potentially modulate neural activity in a precise and localized manner, opening up new avenues for treating neurological disorders and enhancing our understanding of neural circuits.

Chapter 4

In Vivo Peripheral Nervous System Modulation

4.1 Introduction

Building upon the promising results from the BLM experiments, the next critical step is to demonstrate the application of our cellular-sized photovoltaic (PV) devices in modulating the peripheral nervous system (PNS) in living animal models. This in vivo validation is essential for assessing the potential of our technology for future clinical applications and bioelectronic medicine.

For this purpose, we have designed acute in vivo experiments targeting the sciatic nerve, a major nerve in the PNS that innervates the muscles of the lower limb. By injecting our PV devices directly into the sciatic nerve, we aim to achieve precise access to the individual fascicles, enabling targeted stimulation and modulation of the nerve fibers.

Two distinct experimental approaches were employed. In the first approach, immediately following the injection procedure, the nerve was exposed, and laser illumination was applied directly to stimulate the nerve fibers. Subsequently, the nerve was extracted for further analysis after completing the stimulation experiment. In the second approach, the incision site was closed after the injection. Three days later, laser illumination was performed transcutaneously for neuromodulation studies, allowing the stimulation to occur through the overlying tissues. The nerve was then extracted at a later time point for evaluation.

4.1.1 Background on the Peripheral Nervous System and Sciatic Nerve Model

The peripheral nervous system (PNS) comprises the nerves and ganglia located outside the central nervous system (brain and spinal cord). The PNS is responsible for transmitting sensory information from the body to the CNS and carrying motor commands from the CNS to the muscles and glands.

In rodent models, such as mice and rats, the sciatic nerve is a major component of the PNS and is widely used for studying peripheral nerve function and modulation. The sciatic nerve originates from the lumbar and sacral plexuses in the lower back and extends down the leg, innervating various muscles in the thigh, calf, and foot [27].

The sciatic nerve is composed of several fascicles, each containing bundles of individual nerve fibers. These fascicles branch out to innervate different muscle groups, including the hamstring muscles (semitendinosus, semimembranosus, and biceps femoris) in the thigh, the gastrocnemius and soleus muscles in the calf, and the plantar interossei muscles in the foot.

A cross-sectional view of the sciatic nerve reveals its intricate structure [28], consisting of the following layers:

1. Epineurium: The outermost connective tissue layer that surrounds the entire nerve bundle.

2. Perineurium: Layers of connective tissue that surround individual nerve fiber bundles (fascicles).

3. Endoneurium: The innermost layer of connective tissue that surrounds individual nerve fibers within each fascicle.

4. Axons: The central core of each nerve fiber, responsible for transmitting electrical signals.

5. Myelin sheath: A fatty, insulating layer that surrounds the axons of some nerve fibers, facilitating faster signal propagation.

By targeting the sciatic nerve in rodent models, we can study the effects of various interventions, such as electrical or optical stimulation, on peripheral nerve function and the resulting muscle responses.

4.2 Experimental Methods

4.2.1 Animal Models

The in vivo experiments were conducted using BALB/c mice as animal models. These rodent models are widely used in biomedical research and provide a suitable platform for studying the peripheral nervous system. The choice of animal model was based on factors such as the size of the sciatic nerve, ease of surgical access, and compatibility with the experimental setup.

4.2.2 Injection System Design

To achieve direct injection of our devices into the sciatic nerve, we designed a specialized injection system tailored for the mouse model. The typical diameter of the mouse sciatic nerve is approximately 800 µm. To penetrate the epineurium layer, we fabricated custom micro-injection pipettes using a Sutter Instruments P-1000 pipette puller. The pipette pulling recipe was optimized to achieve an outer diameter of 150 µm, ensuring that the devices would not clog the pipette during injection.

The injection pipette was mounted on a pipette holder and integrated with a microprocessor-controlled injection system (Nanoliter 2010, World Precision Instruments, Sarasota, FL, USA). This system allowed for precise control over the injection volume and rate. To further enhance the accuracy of the injection procedure, the entire injection setup was mounted on a micromanipulator system, enabling precise positioning and control of the pipette during the nerve injection process.

4.2.3 Surgical Procedure

1. Anesthesia Induction: On the day of the procedure, general anesthesia was administered to the mice using an isoflurane vaporizer system. The mice were placed in an induction chamber with 2% isoflurane to induce unconsciousness. Confirmation of adequate anesthesia depth was ensured by the absence of a withdrawal reflex upon a toe pinch stimulus.

2. Surgical Preparation: With the mice under general anesthesia, ophthalmic ointment was applied to the eyes to prevent dryness during the procedure. The anesthetized animal was positioned in a ventral recumbency, and the limbs were gently secured using hypoallergenic adhesive tape, creating a mild tension in the limb designated for injection. Anesthesia was maintained via a precision vaporizer and nose cone delivery of isoflurane.

3. Aseptic Technique: The surgical site was prepared aseptically. The area was clipped and alternately scrubbed with Betadine and 70% isopropyl alcohol solutions in a minimum of three alternating cycles. Any remaining loose hair was removed to ensure a clean surgical field.

4. Surgical Approach: A 1 cm skin incision was made approximately 2 mm below and parallel to the femur using surgical scissors. The skin was retracted laterally to expose the underlying musculature. The sciatic nerve was accessed by separating the gluteus maximus and biceps femoris muscles along their fascial plane using blunt dissection techniques. The nerve was carefully isolated from the surrounding muscle tissue.

5. Device Injection: A small metal spatula was positioned beneath the exposed sciatic nerve at the intended injection site to provide support and stabilization. Under microscopic visualization, the injection pipette containing the device suspension was inserted into the nerve bundle, maintaining a parallel orientation to the nerve's longitudinal axis. Care

was taken not to puncture through the opposite side of the nerve. The injection volume of 5 µl was administered at controlled rates ranging from 10 nl/s to 100 nl/s using the microprocessor-controlled injection system. The pipette was left in place for 30 seconds post-injection to minimize backflow before gentle withdrawal.

6. Closure: Upon completion of the injection, the nerve was carefully repositioned, and the overlying muscles were reapproximated to cover the injection site. Appropriate analgesic agents were administered, and the skin incision was closed using 5-0 Nylon sutures.

4.2.4 Sciatic Nerve Extraction

1. Euthanasia: The mice were humanely euthanized using carbon dioxide asphyxiation, following approved protocols.

2. Dissection: The euthanized mouse was positioned in a ventral recumbency, and the distal limbs were secured using pins to facilitate exposure. A dorsal skin incision was made along the injected limb and torso to expose the underlying musculature.

3. Nerve Isolation: The sciatic nerve was identified and carefully dissected free from the surrounding tissues using blunt dissection techniques. The nerve was traced distally to the level of the femur and proximally towards the spinal cord.

4. Spinal Access: To access the proximal extent of the sciatic nerve at the spinal cord level, the ilium and sacrum were separated by inserting closed surgical scissors into the narrow space where the nerve exits and gently spreading the blades.

5. Nerve Harvest: The sciatic nerve was harvested by first transecting the distal end, followed by careful elevation and freeing from adjacent tissues along its length. The proximal end was then transected as close as possible to the spinal cord exit point. Caution was exercised during handling, as invaded nerves are fragile and prone to damage under tension or excessive manipulation.

Following the nerve extraction procedure, the harvested sciatic nerve was subjected to further analyses to evaluate the success of device injection, distribution, and the impact on nerve function and muscle responses, it will be further explained in Nerve Imaging section.

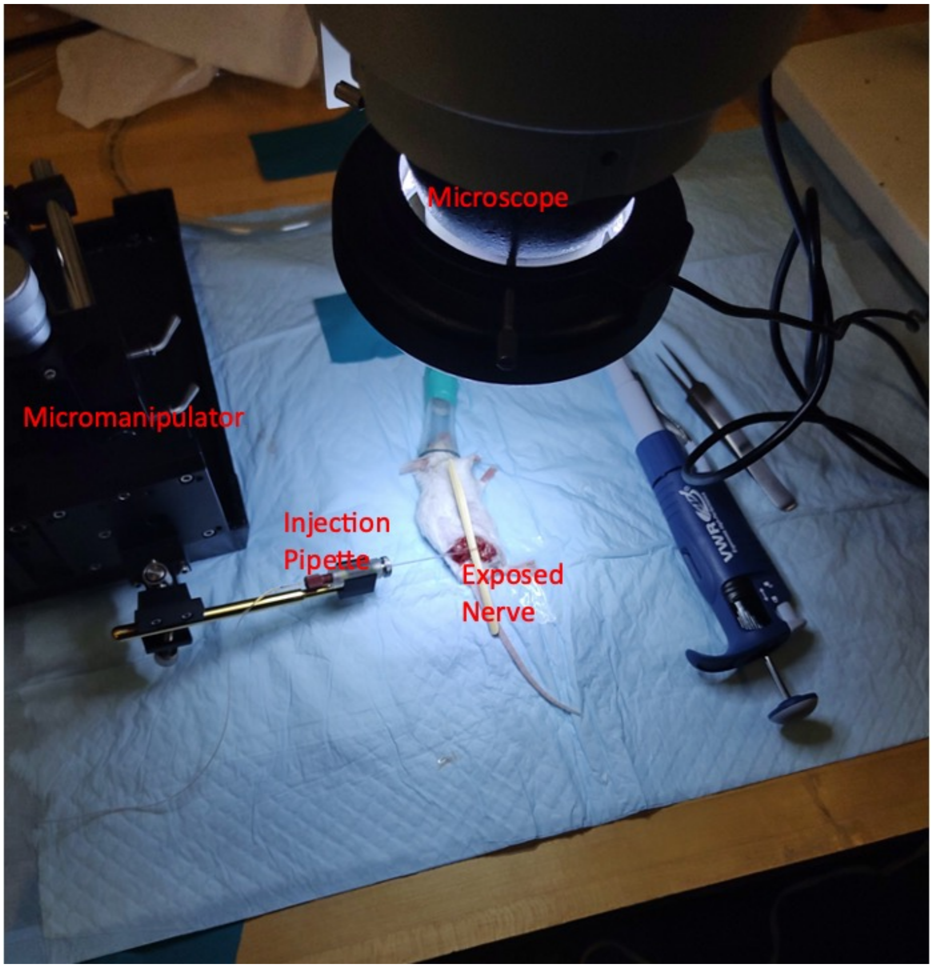

Figure 4-1: Mice Sciatic Nerve Device Injection Setup

4.2.5 Experimental Setups

Two experimental setups were employed to investigate the stimulation capabilities of our PV devices:

1. Direct Laser Stimulation: In this setup, a class IV 895nm laser with a fiber optic and variable diameter collimator ranging from 5mm to 10mm was directed onto the exposed sciatic nerve, allowing for direct illumination of the injected PV devices. This approach

enabled the direct stimulation of the devices within the nerve bundle.

2. Transcutaneous Laser Stimulation: In the second setup, the laser beam was focused through the skin, muscle, and fat tissues surrounding the sciatic nerve. This approach mimicked a more clinically relevant scenario, where non-invasive stimulation is desired. The ability to stimulate the nerve fibers through the overlying tissues was evaluated using electrophysiology recordings, as explained in the following sections.

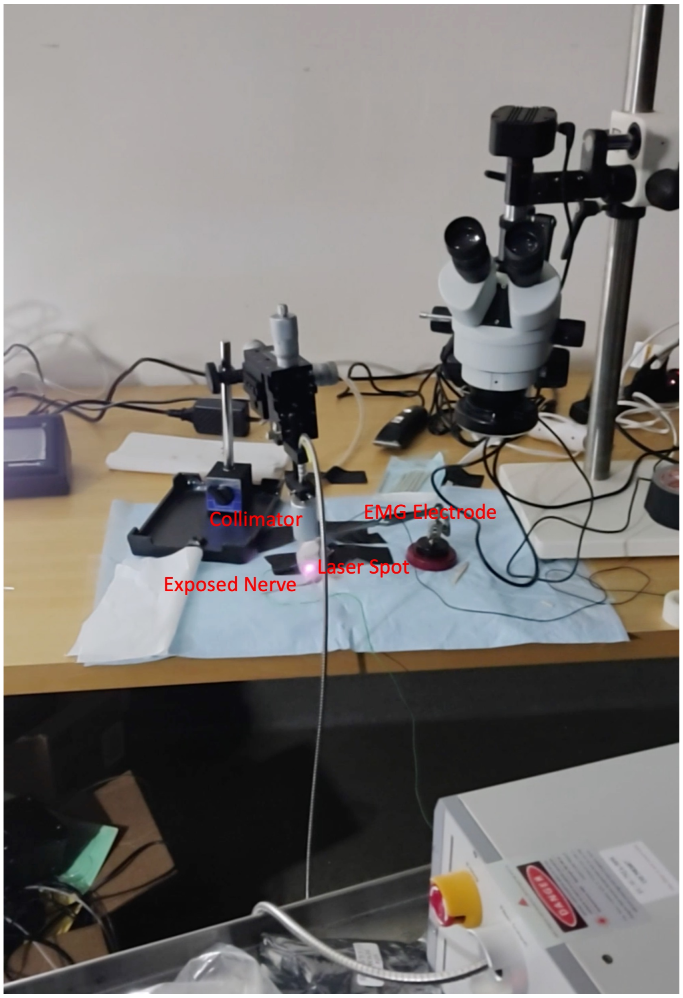

Figure 4-2: Laser Illuminations and EMG Recording post Nerve Injection

4.2.6 Electrophysiological Recordings

To record the compound muscle action potentials (CMAPs) and characterize the stimulation response, electromyography (EMG) electrodes were placed in the biceps femoris and plantar muscles innervated by the sciatic nerve. The in vivo stimulation characterization was performed using a multichannel EMG machine from Tucker Davis Technologies.

The EMG recordings provided insights into the muscle activation patterns and the selectivity of stimulation achieved by our PV devices. By monitoring the electrical activity in the target muscles, we were able to assess the efficacy of our devices in eliciting neural responses and the potential for selective nerve fiber recruitment.

The multichannel EMG system allowed for simultaneous recordings from multiple muscle groups, enabling a comprehensive evaluation of the stimulation effects on the sciatic nerve and its associated motor pathways.

4.3 Results, Discussion and Future Directions

The electrophysiological recordings from the biceps femoris and plantar muscles did not show robust stimulation responses as anticipated. The compound muscle action potentials (CMAPs) elicited by the PV devices were variable and generally weaker than expected. This suggests that the devices were not effectively integrated or distributed within the nerve tissue, limiting their ability to efficiently stimulate the target nerve fibers.

The imaging evaluation of the harvested sciatic nerve revealed an uneven distribution pattern of the injected devices within the nerve bundle for the stimulation cohort animals. The gross length of nerve invasion by the devices was lower than desired, indicating that the injection process may have been suboptimal in achieving a consistent and widespread distribution throughout the nerve fascicles.

4.3.1 Nerve Imaging and Device Distribution Analysis

To visualize the three-dimensional distribution of the injected devices within the mouse sciatic nerve, we employed advanced imaging techniques in conjunction with a tissue transparency protocol. The typical diameter of the mouse sciatic nerve is approximately 800 µm, which poses challenges for conventional imaging methods. Sectioning the nerve could potentially disrupt the delicate distribution of the devices, while the limited optical penetration depth of confocal microscopy restricts the ability to image the entire nerve thickness.

To overcome these limitations, we adopted a tissue transparency protocol based on the work of Xu et al [29], Fast Optical Clearing Method (FOCM). This protocol involves a series of steps to render the nerve tissue optically transparent, enabling high-resolution imaging of the entire nerve depth without the need for physical sectioning. The protocol was implemented as follows:

1. Fixation: The transected sciatic nerve was fixed in 4% paraformaldehyde (PFA) for 5 hours at 4°C to preserve the tissue structure.

2. Washing: The fixed nerve was washed three times for 1 minute each in 0.01M phosphate-buffered saline (PBS) at room temperature to remove residual PFA.

3. Incubation: The nerve was incubated in 0.01M PBS for 30 minutes at room temperature to further remove any remaining PFA.

4. Storage (optional): If immediate processing was not required, the nerve could be stored in an antifreeze solution (equal volumes of glycerol and 0.01M PBS) at -20°C for up to a month.

5. Clearing: The nerve was incubated in a clearing solution called FOCM (30% urea, 20% d-sorbitol, 5% glycerol in DMSO) for 1-5 minutes at room temperature with gentle shaking.

6. Mounting: After the clearing process, the transparent nerve samples were mounted for confocal imaging.

The FOCM clearing reagent was prepared by dissolving urea and d-sorbitol in DMSO and stirring overnight at room temperature. Glycerol was then added, and the solution was further stirred. This reagent can be stored at room temperature for several months and gently shaken before use.

By following this tissue transparency protocol, we successfully rendered the mouse sciatic nerve optically transparent, enabling us to image the entire nerve depth using confocal microscopy without the need for two-photon microscopy. The transparency of the nerve was so remarkable that we could visualize the distribution of the injected devices throughout the nerve bundle using confocal imaging alone.

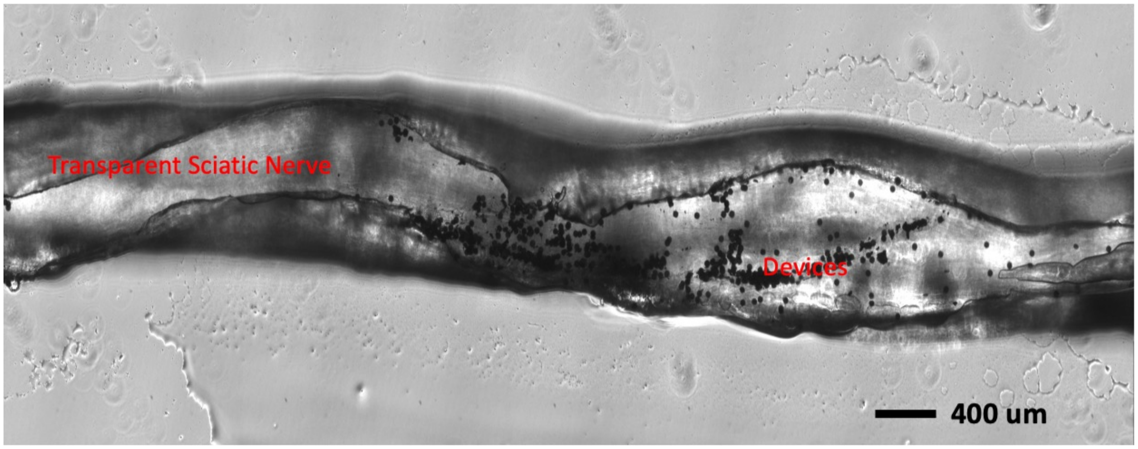

Figure 4-3: Confocal Image of Transected Nerve post device injection and transparency protocol

Figure 4-3 and 4-4 shows devices embedded deep inside the nerve, making the nerve transparent allows imaging the whole depth of the nerve using a confocal microscope without sectioning the nerve and gives complete idea of 3D spatial distribution of devices inside the nerve.

The confocal images of the transparent nerve samples provided valuable insights into the distribution pattern of the injected devices within the nerve fascicles. These images allowed us to assess the success of the injection process and identify areas where the devices were successfully integrated or where further optimization might be required.

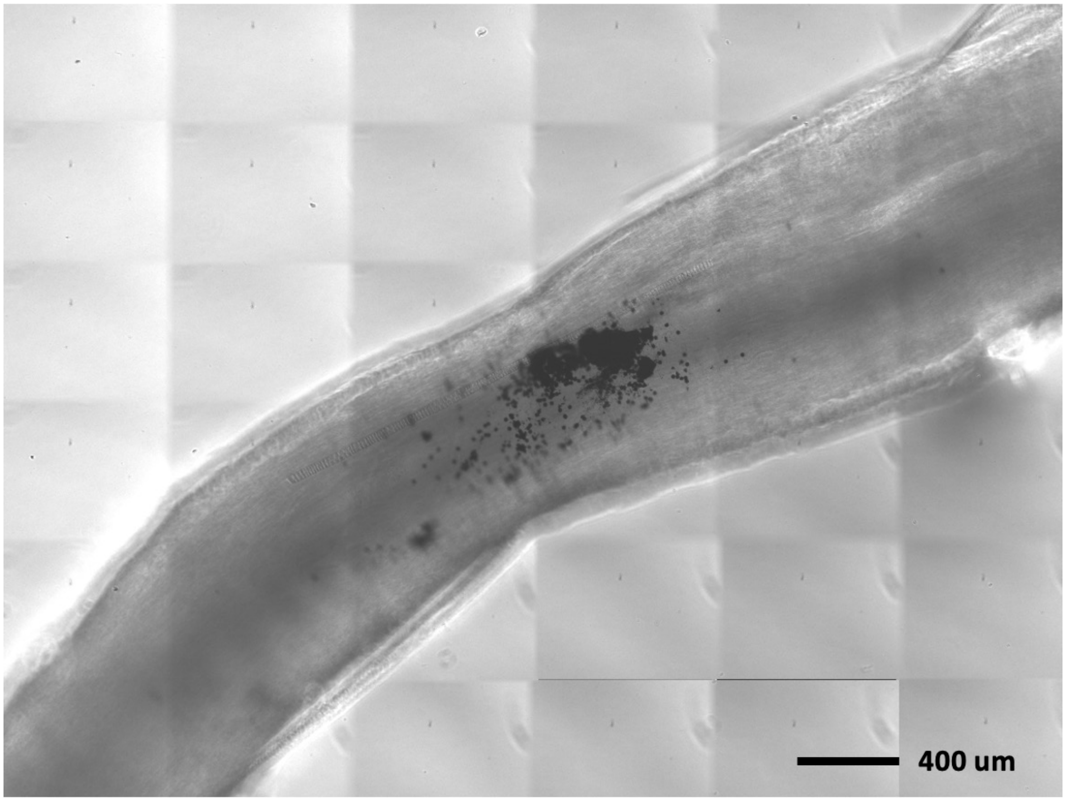

Figure 4-4: Confocal Image of Transected Nerve post device injection and transparency protocol

4.3.2 Discussion

The nerve imaging results shed light on a significant challenge encountered in the current approach. The low density and uneven distribution of the injected devices within the nerve tissue likely contributed to the suboptimal stimulation responses observed in the electrophysiological recordings.

The ability to effectively stimulate and modulate the peripheral nervous system relies on the successful integration and widespread distribution of the PV devices throughout the nerve fascicles. The observed sparse distribution and localized clustering of devices within the nerve bundle may have limited their ability to efficiently stimulate the target nerve fibers, resulting in the weaker and variable CMAPs recorded.

Additionally, the variability in the injection process itself may have played a role in the in-consistent results. Factors such as the injection rate, needle positioning, and nerve handling during the procedure could have influenced the distribution and integration of the devices within the nerve tissue.

4.3.3 Future Work

To address the challenges identified in this study, future efforts should focus on optimizing the injection procedure to achieve a more consistent and widespread distribution of the PV devices within the nerve bundle. Potential strategies include:

1. Refining the injection system and parameters: Exploring different injection rates, volumes, and needle geometries to enhance the dispersion of devices throughout the nerve fascicles.

2. Developing new injection techniques: Investigating alternative methods, such as multiple injection sites or the use of specialized delivery vehicles, to improve the distribution and integration of devices within the nerve tissue.

3. Improving device design: Exploring modifications to the device size, shape, or surface properties to facilitate better integration and distribution within the nerve environment.

4. Conducting additional imaging studies: Utilizing advanced imaging techniques, such as light-sheet microscopy or micro-computed tomography (micro-CT), to gain a more comprehensive understanding of the device distribution patterns within the nerve tissue.

5. Expanding the animal model: Evaluating the injection and stimulation procedures in larger animal models with larger nerve diameters to assess the scalability and translational potential of the approach.

By addressing these challenges and optimizing the injection and device integration processes, future studies may achieve more consistent and robust stimulation responses.

Chapter 5

Conclusions and Future Work

5.1 Conclusions

This work has demonstrated the potential of injectable electronics for minimally invasive and precise neuromodulation of the peripheral nervous system (PNS). Through the development of highly efficient, wireless, cellular-sized photovoltaic (PV) devices, we have overcome several limitations of current implantable technologies, paving the way for a transformative approach to bioelectronic medicine.

The following have been achieved in this work:

1. Successful fabrication of freestanding, injectable PV devices with dimensions as small as 10 µm, enabling access to individual nerve fascicles and axons.

2. Optimization of device architecture and material selection, including the use of PEDOT:PSS, organic semiconducting polymers, titanium, and titanium nitride, to enhance biocompatibility, charge generation, and neural stimulation capabilities.

3. Comprehensive characterization of device performance, demonstrating their ability to generate sufficient voltage changes across neuronal membranes for neuromodulation under safe light intensities.

4. Validation of device functionality in a biologically relevant environment through lipid bilayer membrane experiments, confirming their potential for neural stimulation applications.

5. Successful in vivo injection of devices into the sciatic nerve of mouse models, showcasing the feasibility of minimally invasive delivery and targeted access to the PNS.

While the in vivo experiments encountered challenges in achieving consistent and widespread device distribution, the findings from this research have laid a solid foundation for the future development of injectable electronics for bioelectronic medicine.

5.2 Future Work

Building upon the achievements of this thesis, future research will be focused on:

1. Injection Technique Optimization: Refine the injection system and parameters, such as needle geometry, injection rates, and delivery vehicles, to enhance the dispersion and integration of devices throughout the nerve fascicles. Explore alternative injection techniques, including multiple injection sites or specialized delivery methods.

2. Device Design Improvements: Investigate modifications to the device size, shape, surface properties, and material composition to facilitate better integration and distribution within the nerve environment. Explore strategies to improve device stability and longevity in biological systems.

3. In Vivo Chronic Studies: Conduct long-term chronic implantation studies to evaluate the biocompatibility, stability, and efficacy of the injectable devices over extended periods. Assess the potential for foreign body responses and develop strategies to mitigate them.

4. Expanded Animal Models: Evaluate the scalability and translational potential of the injectable electronics technology by conducting studies in larger animal models with larger nerve diameters, such as rats or non-human primates.

5. Closed-Loop Neuromodulation Systems: Integrate the injectable PV devices with advanced sensing and feedback control systems to enable closed-loop neuromodulation, allowing for real-time monitoring and adaptive stimulation based on physiological signals.

By addressing these future directions, the field of injectable electronics can continue to evolve, unlocking new possibilities for minimally invasive, targeted, and personalized neuromodulation therapies. The successful translation of this technology could revolutionize the way we diagnose, treat, and manage a wide range of neurological disorders, ultimately improving the quality of life for countless individuals.

Bibliography

[1] Sandro Carrara and Krzysztof Iniewski. Handbook of bioelectronics: Directly interfacing electronics and biological systems. *Handbook of Bioelectronics: Directly Interfacing Electronics and Biological Systems*, pages 1–577, 1 2015.

[2] Patricia Jastrzebska-Perfect, Shilpika Chowdhury, George D Spyropoulos, Zifang Zhao, Claudia Cea, Jennifer N Gelinas, Dion Khodagholy, P Jastrzebska-Perfect, S Chowdhury, G D Spyropoulos, Z Zhao, C Cea, D Khodagholy, and J N Gelinas. Translational neuroelectronics. *Advanced Functional Materials*, 30:1909165, 7 2020.

[3] Andres M. Lozano, Nir Lipsman, Hagai Bergman, Peter Brown, Stephan Chabardes, Jin Woo Chang, Keith Matthews, Cameron C. McIntyre, Thomas E. Schlaepfer, Michael Schulder, Yasin Temel, Jens Volkmann, and Joachim K. Krauss. Deep brain stimulation: current challenges and future directions. *Nature Reviews Neurology 2019 15:3*, 15:148–160, 1 2019.

[4] Alice T. Chuang, Curtis E. Margo, and Paul B. Greenberg. Retinal implants: a systematic review. *British Journal of Ophthalmology*, 98:852–856, 7 2014.

[5] Rhaya L. Johnson and Christopher G. Wilson. A review of vagus nerve stimulation as a therapeutic intervention. *Journal of Inflammation Research*, 11:203–213, 5 2018.

[6] E. Ben-Menachem, D. Revesz, B. J. Simon, and S. Silberstein. Surgically implanted and non-invasive vagus nerve stimulation: a review of efficacy, safety and tolerability. *European Journal of Neurology*, 22:1260–1268, 9 2015.

[7] April S. Caravaca, Alessandro L. Gallina, Laura Tarnawski, Kevin J. Tracey, Valentin A. Pavlov, Yaakov A. Levine, and Peder S. Olofsson. An effective method for acute vagus nerve stimulation in experimental inflammation. *Frontiers in Neuroscience*, 13:472472, 8 2019.

[8] Karen Birmingham, Viviana Gradinaru, Polina Anikeeva, Warren M. Grill, Victor Pikov, Bryan McLaughlin, Pankaj Pasricha, Douglas Weber, Kip Ludwig, and Kristoffer Famm. Bioelectronic medicines: a research roadmap. *Nature Reviews Drug Discovery 2014 13:6*, 13:399–400, 5 2014.

[9] Héctor Acarón Ledesma, Xiaojian Li, João L. Carvalho de Souza, Wei Wei, Francisco Bezanilla, and Bozhi Tian. An atlas of nano-enabled neural interfaces. *Nature Nanotechnology 2019 14:7*, 14:645–657, 7 2019.

[10] Peter M. Miller and Robert E. Gross. Wire tethering or 'bowstringing' as a long-term hardware-related complication of deep brain stimulation. *Stereotactic and Functional Neurosurgery*, 87:353–359, 11 2009.

[11] Benjamin S. Spearman, Vidhi H. Desai, Sahba Mobini, Matthew D. McDermott, James B. Graham, Kevin J. Otto, Jack W. Judy, and Christine E. Schmidt. Tissue-engineered peripheral nerve interfaces. *Advanced Functional Materials*, 28:1701713, 3 2018.

[12] Hayriye Cagnan, Timothy Denison, Cameron McIntyre, and Peter Brown. Emerging technologies for improved deep brain stimulation. *Nature Biotechnology 2019 37:9*, 37:1024–1033, 9 2019.

[13] David K. Piech, Benjamin C. Johnson, Konlin Shen, M. Meraj Ghanbari, Ka Yiu Li, Ryan M. Neely, Joshua E. Kay, Jose M. Carmena, Michel M. Maharbiz, and Rikky Muller. A wireless millimetre-scale implantable neural stimulator with ultrasonically powered bidirectional communication. *Nature Biomedical Engineering 2020 4:2*, 4:207–222, 2 2020.

[14] Ritchie Chen, Gabriela Romero, Michael G. Christiansen, Alan Mohr, and Polina Anikeeva. Wireless magnetothermal deep brain stimulation. *Science*, 347:1477–1480, 3 2015.

[15] Adam Khalifa, Yuxin Liu, Yasha Karimi, Qihong Wang, Adebayo Eisape, Milutin Stanaćević, Nitish Thakor, Zhenan Bao, and Ralph Etienne-Cummings. The microbead: A 0.009 mm3 implantable wireless neural stimulator. *IEEE Transactions on Biomedical Circuits and Systems*, 13:971–985, 10 2019.

[16] Kaylene C. Stocking, Alberto L. Vazquez, and Takashi D.Y. Kozai. Intracortical neural stimulation with untethered, ultrasmall carbon fiber electrodes mediated by the photoelectric effect. *IEEE Transactions on Biomedical Engineering*, 66:2402–2412, 8 2019.

[17] Thomas Stieglitz. Why neurotechnologies? about the purposes, opportunities and limitations of neurotechnologies in clinical applications. *Neuroethics*, 14:5–16, 4 2021.

[18] David M. Sokal, Alex McSloy, Matteo Donegà, Joseph Kirk, Romain A. Colas, Nikola Dolezalova, Esteban A. Gomez, Isha Gupta, Cathrine T. Fjordbakk, Sebastien Ouchouche, Paul B. Matteucci, Kristina Schlegel, Rizwan Bashirullah, Dirk Werling, Kim Harman, Alison Rowles, Refet Firat Yazicioglu, Jesmond Dalli, Daniel J. Chew, and Justin D. Perkins. Splenic nerve neuromodulation reduces inflammation and promotes resolution in chronically implanted pigs. *Frontiers in Immunology*, 12:649786, 3 2021.

[19] David G. Armstrong, Lawrence A. Lavery, John G. Fleischli, and Karry Ann Gilham. Is electrical stimulation effective in reducing neuropathic pain in patients with diabetes? *The Journal of Foot and Ankle Surgery*, 36:260–263, 7 1997.

[20] Matija Milosevic, Cesar Marquez-Chin, Kei Masani, Masayuki Hirata, Taishin Nomura, Milos R. Popovic, and Kimitaka Nakazawa. Why brain-controlled neuroprosthetics matter: mechanisms underlying electrical stimulation of muscles and nerves in rehabilitation. *BioMedical Engineering OnLine*, 19, 12 2020.

[21] Jean Luc Bredas and James R. Durrant. Organic photovoltaics. *Accounts of Chemical Research*, 42:1689–1690, 11 2009.

[22] Chuanwang Yang, Zhe Cheng, Pengju Li, and Bozhi Tian. Exploring present and future directions in nano-enhanced optoelectronic neuromodulation. *Accounts of Chemical Research*, 57:9, 2024.

[23] Yuanying Liang, Andreas Offenhäusser, Sven Ingebrandt, Dirk Mayer, Y Liang, A Offenhäusser, D Mayer, and S Ingebrandt. Pedot:pss-based bioelectronic devices for recording and modulation of electrophysiological and biochemical cell signals. *Advanced Healthcare Materials*, 10:2100061, 6 2021.

[24] Kaitlynn P Olczak and Kevin John Otto. Performance of titanium nitride electrodes used for chronic peripheral nerve stimulation. *ECS Meeting Abstracts*, MA2020-02:1576, 11 2020.

[25] Naser Pour Aryan, Mohammad Imam Hasan Bin Asad, Christian Brendler, Steffen Kibbel, Gerhard Heusel, and Albrecht Rothermel. In vitro study of titanium nitride electrodes for neural stimulation. *Proceedings of the Annual International Conference of the IEEE Engineering in Medicine and Biology Society, EMBS*, pages 2866–2869, 2011.

[26] Lingyan Shi, Laura A. Sordillo, Adrián Rodríguez-Contreras, and Robert Alfano. Transmission in near-infrared optical windows for deep brain imaging. *Journal of Biophotonics*, 9:38–43, 1 2016.

[27] Martin Catala and Nathalie Kubis. Gross anatomy and development of the peripheral nervous system. *Handbook of Clinical Neurology*, 115:29–41, 1 2013.

[28] H. Schmalbruch. Fiber composition of the rat sciatic nerve. *The Anatomical Record*, 215:71–81, 5 1986.

[29] Xinpei Zhu, Limeng Huang, Yao Zheng, Yanchun Song, Qiaoqi Xu, Jiahao Wang, Ke Si, Shumin Duan, and Wei Gong. Ultrafast optical clearing method for three-dimensional imaging with cellular resolution. *Proceedings of the National Academy of Sciences of the United States of America*, 166:11480–11489, 6 2019.